Analysis of the behavior in a squirrel cage motor under electrical internal fault

D. A. Aguilar Arévalo, H. D. Puin Ávila and H. E. Ortiz Suarez
Universidad Distrital Francisco José de Caldas, Ingeniería Eléctrica, Bogotá D.C., Colombia

***Abstract*—The continuous and intensive use of squirrel-cage induction motors in the modern industry, has in some cases caused a serious deterioration of the electrical insulation in the windings of the machine, generating as a consequence internal short-circuit failures, the effects on the operation of the machine are difficult to determine experimentally.**

In this paper is presented a 2D model, time dependent on an induction motor 1.1 KW, which implements a coupling of the interfaces of rotating machines, electrical circuits and global ODEs and DAEs of COMSOL Multiphysics ® to determine the behavior of current, voltage, distribution of magnetic flux, magnetic field density, torque and speed in the transition from normal operation to operation under internal short-circuit failure of adjacent phase coils.

The model has three different levels of short-circuit severity, performing a comparative analysis with the model in normal operation, the latter validated with experimental results.

***Keywords*— Induction motor, internal electrical failures, short-circuit, field magnetic fault, current fault.**

I. INTRODUCTION

The squirrel cage induction motor is one of the most versatile electric machines of today, due to technical characteristics such as low maintenance cost, high reliability, high efficiency and high starting torque [1], being implemented in about 70 % of the global industry, consuming approximately 50% of the energy produced on the planet [2]. However, the continuous use of these machines can lead to premature wear in the electrical insulation of their windings, generating short circuit failures, causing their definitive exit from service [3].

There are different types of internal short circuit failures [4] [5], however this article will focus on determining the mechanical, magnetic and electrical effects on the operation of an squirrel cage induction motor that is subjected to a fault of internal short circuit of two adjacent phases [6], under three levels of severity, by 2D FEM analysis, time dependent on COMSOL Multiphysics ® v5.3.

The development of this document, initially presents in section II the technical characteristics of the engine under analysis, in section III is detailed the modeling and simulation process, for which the AC / DC and mathematics modules have been jointly implemented of COMSOL Multiphysics ® v5.3a, section IV performs a validation of the mechanical and electrical behavior of the motor in normal operation obtained in the simulation, with the experimentally obtained, in section V the simulated results are presented in a comparative manner of the behavior of electrical, magnetic and mechanical variables in the motor under the three levels of severity of the fault. Finally, the analysis of results and conclusions are presented in sections VI and VII respectively.

II. MOTOR CHARACTERISTICS

A. Technical Plate

Fig 1.Generic motor NEMA class B of 1.1KW.
Source: Author's own elaboration

The motor object of this study corresponds to a three-phase induction motor NEMA Squirrel Cage class B of 1.1 KW illustrated in Fig. 1, whose characteristics are in Table I.

TABLE I. CHARACTERISTICS MOTOR OBJECT OF STUDY.

Parámetro	Unidad	Valor
Voltage Δ/Y	V	220 / 380
Current Δ/Y	A	4.7 / 2.7
Frecuency	Hz	60
Power	kW	1.1
Power factor Φ	-	0.9
Number of poles	-	2
Nominal velocity	rpm	3350
Nominal torque	Nm	3.05
Stator external radio	cm	6.180
Stator internal radio	cm	3.622
Rotor external radio	cm	3.522
Air gap	mm	1
Number of stator slots	-	18
Stator slot area	mm^2	48
Ring thickness in the rotor	cm	2
Coils per phase group	-	3
Poles	-	2

B. Configuration windings

The stator of the machine has double-layer windings, two poles, 6 coils per phase, divided into 3 coils for each of the two phase groups, with a slot range (γ) of 20 ° electrical, connected in series and distributed in the stator according to what is shown in Fig. 2.

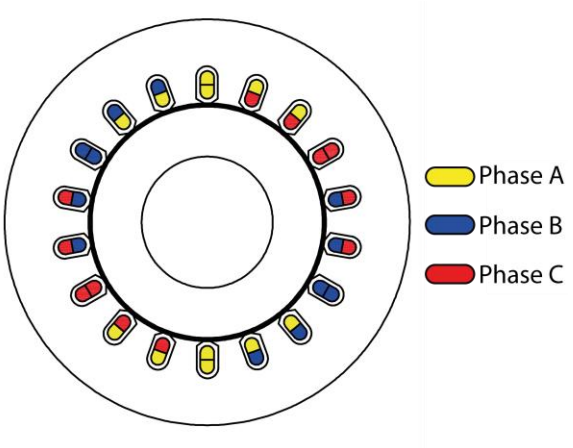

Fig 2. Distribution by phase of the motor coils
Source: Author's own elaboration.

C. *Engine type tests.*

Table II presents the test values to determine the equivalent model of the motor.

TABLE II. DATA OF THE MOTOR TYPE TESTS

Test	Parameter	Unity	Value
Stator resistor	R	Ω	15.23
Rotor blocked	Vrb	V	96.1
	Irb	A	2.70
	Prb	W	281
Mechanical losses	Pmec	W	81.64
Empty	Vo	V	380.7
	Io	A	1.00
	Po	W	169

*The parameters were measured with the motor in Y connection.

III. MODELING AND SIMULATION PROCESS

In the modeling wizard of COMSOL Multiphysics ® v5.3, a 2D-time-dependent study geometry was initially established, selecting the interfaces of rotating machinery and electrical circuit of the AC / DC module, as well as the global interface ODEs and DAEs of the Math module.

A. *Parameters and variables*

The parameters established for the model are presented in Table III. Similarly, in table IV, the density of the materials of the iron and the aluminum ring of the rotor, multiplied by a factor K1 and K2 respectively, was defined for the model in the form of variables, with the objective of representing the stresses caused for bearings and losses due to friction with the wind.

TABLE III. LOCAL PARAMETERS.

Name	Expression	Value	Description
f0	60 [Hz]	60 Hz	Frecuencia
w0	2*pi*f0	376.99 rad/s	Frecuencia angular
no	225	225	Turns
L	7.32[cm]	0.0732 m	Length
airgap	1[mm]	0.001 m	Airgap
RF	2[Ω]	2 Ω	Source resistance

TABLE IV. VARIABLES.

Name	Expression	Unity	Description
rho_Fe	7850 * K_1 [Kg/m^3]	Kg/m^3	Consistencia del hierro en el rotor
rho_Al	2700 * K_2 [Kg/m^3]	Kg/m^3	Consistencia del aluminio en el rotor

For the calculation of the torque generated by the motor, it was implemented in the arkkio method from its mathematical definition made in the form of a variable in the model.

B. *Geometry and materials*

The geometric two-dimensional modeling of each component of the engine was carried out by implementing the CAD design tools that COMSOL Multiphysics ® v5.3 possesses, as shown in figure 3. The geometry was consolidated by forming an assembly creating an identity pair that separates the dynamic part of the static part of the engine. The material selected for each section is listed in table V.

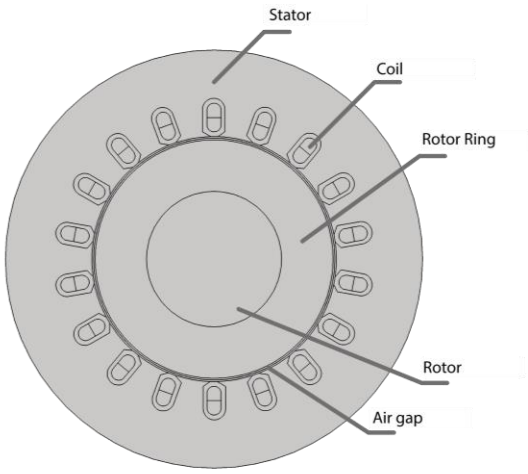

Fig 3. Two-dimensional geometry of the motor object of study.
Source: Author's own elaboration.

TABLE V. MATERIALS USED IN THE FEM MODEL.

Part	Material
Stator	Soft iron (Without losses)
Windings	Copper
Rotor ring	Aluminum
Rotor	Soft iron (Without losses)
Airgap	Air

C. *Global ODEs and DAEs configuration*

This interface is configured, so that from the data calculated by the arkkio method the angular frequency W in [rad / s] and the angle phi of rotation of the rotor in [°], determined by the establishment of the global equations, shown in (1)

$$W = d(W,t) - \frac{T_{ark} - T_{Load}}{I_{rotor}}, \qquad phi = d(phi,t) - W \quad (1)$$

D. *Rotating machinery configuration*

The magnetic field in the stator and rotor of the motor is generated from the implementation per phase, of 12 coil

domains, divided into 2 groups of 6 for the generation of two diametrically opposed magnetic poles, the rotation of the motor is achieved by the use of a domain of the prescribed rotation that has as an assigned variable of rotation, to phi, whose calculation procedure was exposed in the previous item. The differential equations established in this interface are presented in (2)

$$\nabla * H = J, \qquad B = \nabla * A, \qquad E = \frac{-\partial A}{\partial t} \qquad (2)$$

E. Electrical circuit configuration

By means of the basic circuit elements that this interface has, such as voltage sources, resistors and inductors and based on the type tests of the motor exposed in item C of section II of this document, the circuit model was established by phase of the machine, as illustrated in figure 4.

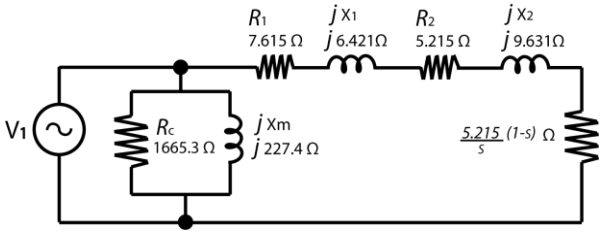

Fig 4. Circuit model by phase of the motor.
Source: Author's own elaboration.

The power supply of the motor circuit was carried out by means of a three-phase alternating voltage source with the parameters established in table VI.

TABLE VI. SOURCE CONFIGURATION.

Name	Expression	Unity	Description
rho_Fe	7850 * K_1 [Kg/m^3]	Kg/m^3	Rotor iron consistence
rho_Al	2700 * K_2 [Kg/m^3]	Kg/m^3	Rotor aluminum consistence

The circuit model generated in this interface is related to the rotating machinery interface, assigning as current value to each of the 12 coil domains the current variable that circulates through 12 resistors of very low ohmic value that are connected in series between the three-phase source and the motor circuit model. In the same way, the slip of the motor linked to the circuit model is established from the calculation of W, obtained in the Global ODEs and DAEs interface. In this way, all the interfaces are coupled and interrelated with each other, which results in a highly accurate behavior of the motor, operating in both normal and fault conditions.

F. Mesh configuration.

A general mesh is established for the model, but emphasizing in the same way with free triangles and boundary layers with fine meshing in the air gap zones and windings. In Fig. 5 the meshing of the model is observed.

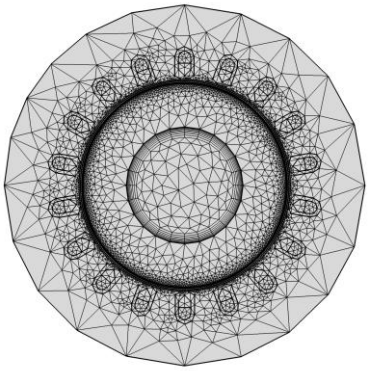

Fig 5. Mesh.
Source: COMSOL Multiphysics.

IV. FEM SIMULATION VALIDATION

The results obtained when the induction motor operates at nominal power in normal state are shown below.

A. Phase current in normal operation.

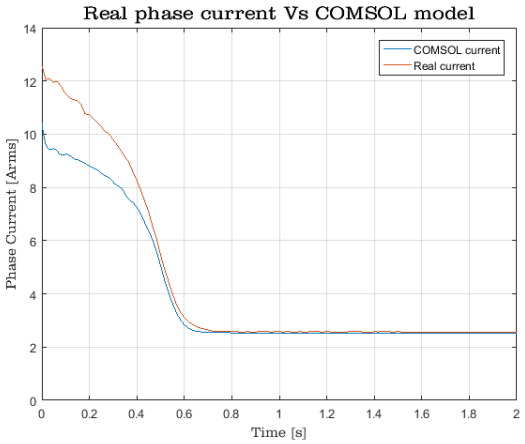

Fig 6. Actual phase current and phase current as a result of modeling in COMSOL.
Source: Author's own elaboration.

Fig. 6 shows the rms value of the starting current per phase as a function of time as a real parameter measured in the laboratory and the result obtained with the FEM model. There is detailed a relative error in the real simulated vs simulated peak current of 16.91%; a relative error of the real current vs simulated steady state of 2.08%; and a relative error of the current stabilization time of 5.94%.

B. Speed in normal operation

Fig. 7 shows the speed (from start to full speed) of the engine, measured in the laboratory and compared to the speed obtained in the FEM model. A similar behavior is shown for both its time and its stabilization value. The greatest relative error occurs at 560 ms with 5.00%, however in steady state the relative error drops to 0.88%.

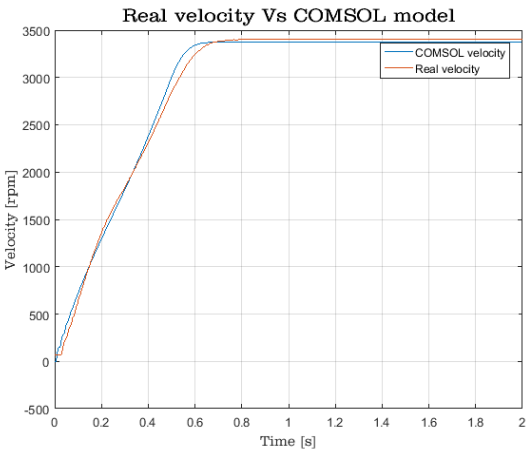

Fig 7. Actual speed and modeling result in COMSOL.
Source: Author's own elaboration.

C. *Torque in normal operation*

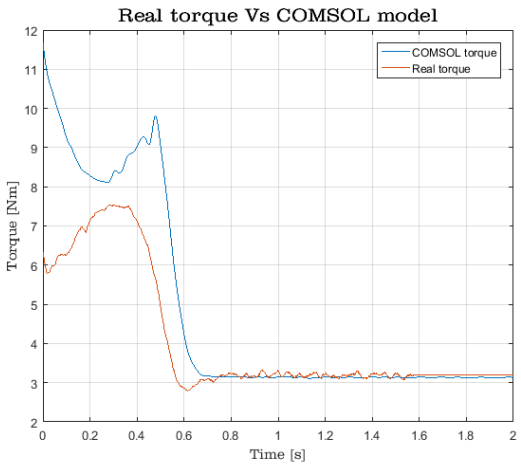

Fig 8. Real torque and modeling result in COMSOL.
Source: Author's own elaboration.

Torque is a variable strongly conditioned by electromagnetic, mechanical and constructive parameters, with which a considerable difference is obtained in terms of the behavior exhibited in the FEM model and the behavior obtained from the real engine, being evident in the transitory state (starting), without However, it is worth noting the similar behavior of the simulated model and the real one in the stable state, since this presents a relative error of 2.64%.

V.FEM SIMULATION OF THE MOTOR UNDER FAULT

The biphasic internal short circuit fault in induction motors, represents the loss of insulation in the coils of adjacent phase coils that share grooves or sections of slot change inside the stator of the motor, typical situation presented in conditions of prolonged overcurrent or overvoltages presented by poor insulation calculation practices in irregular preventive maintenance procedures or engine operation.

Fig. 9, 10 and 11, schematizes electrically the two windings in fault (Phase a and c) and the corresponding percentage of affectation for each one.

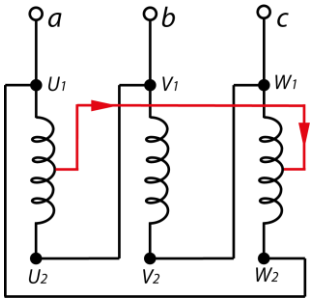

Fig 9. Electrical diagram, fault between phase coils, with percentage of 50-50 affectation.
Source: Author's own elaboration.

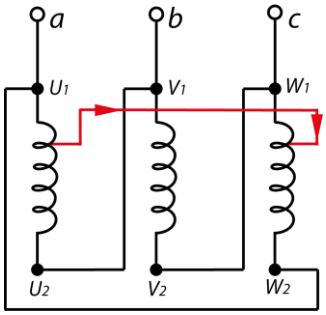

Fig 10. Electrical diagram, fault between phase coils, with percentage of 80-80 affectation.
Source: Author's own elaboration.

.

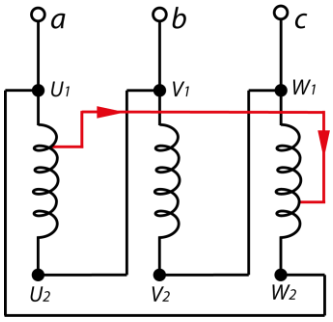

Fig 11. Electrical diagram, fault between phase coils, with percentage of 70-10 affectation.
Source: Author's own elaboration.

Next in fig 12, 13 and 14, the results of the behavior of the current are presented, in the transition from normal operation to operation under engine failure, the three failure scenarios are low.

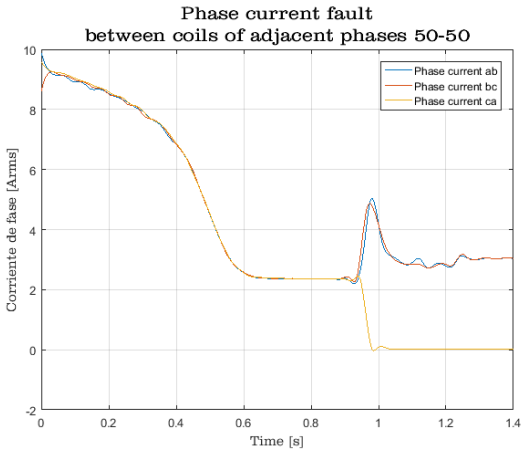

Fig 12. Current - fault between coils of adjacent phases 50-50.
Source: Author's own elaboration.

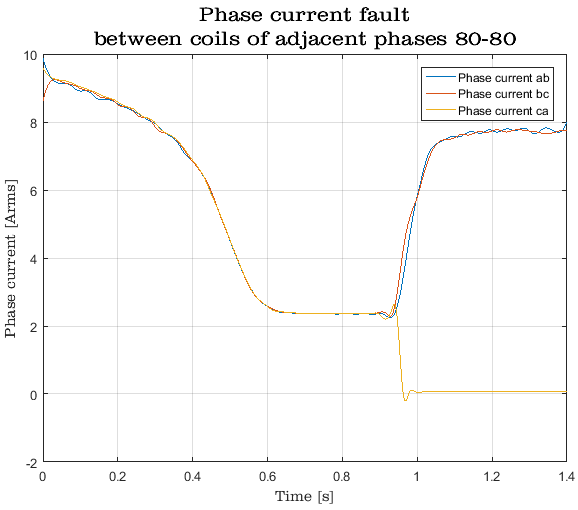

Fig 13. Current - fault between coils of adjacent phases 80-80.
Source: Author's own elaboration.

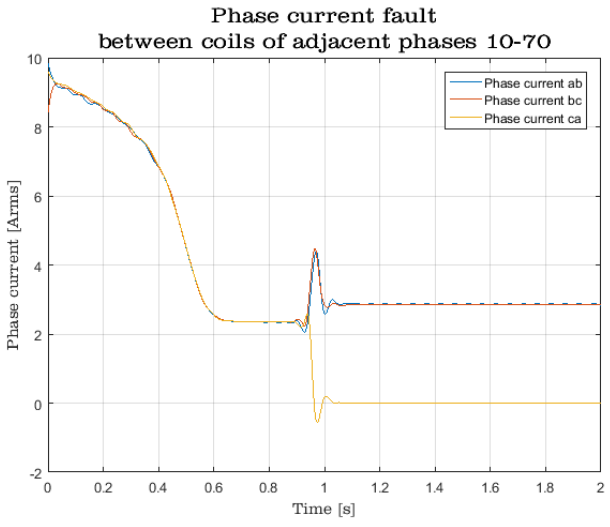

Fig 14. Current - fault between coils of adjacent phases 10-70.
Source: Author's own elaboration.

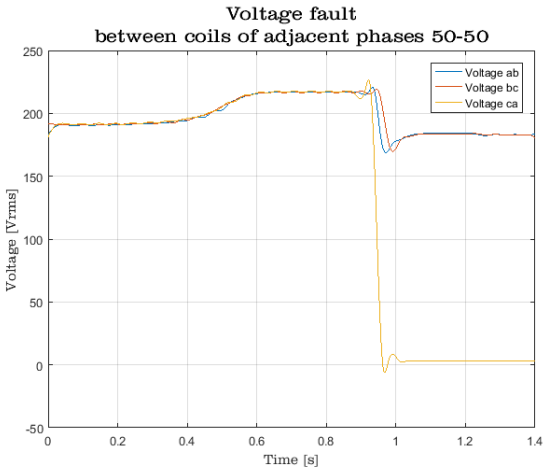

Fig 15. Voltage - fault between coils of adjacent phases 50-50.
Source: Author's own elaboration.

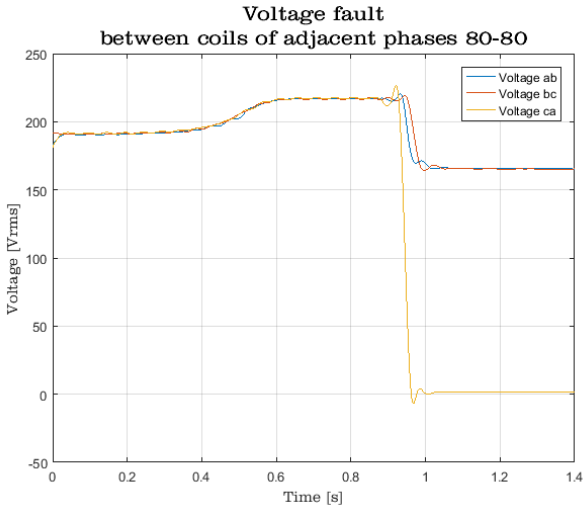

Fig 16. Voltage - fault between coils of adjacent phases 80-80.
Source: Author's own elaboration.

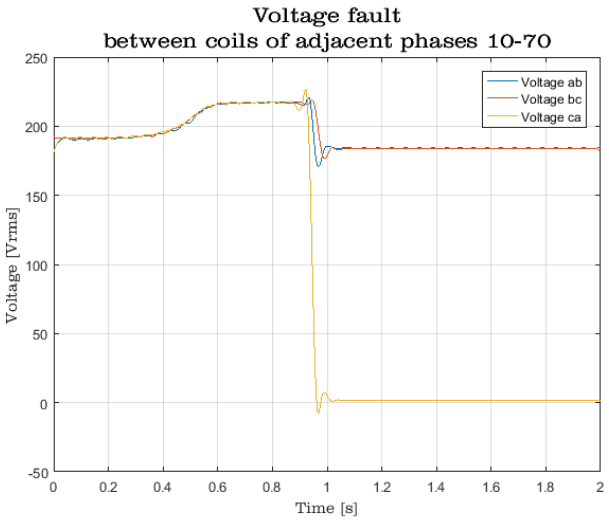

Fig 17. Voltage - fault between coils of adjacent phases 10-70.
Source: Author's own elaboration.

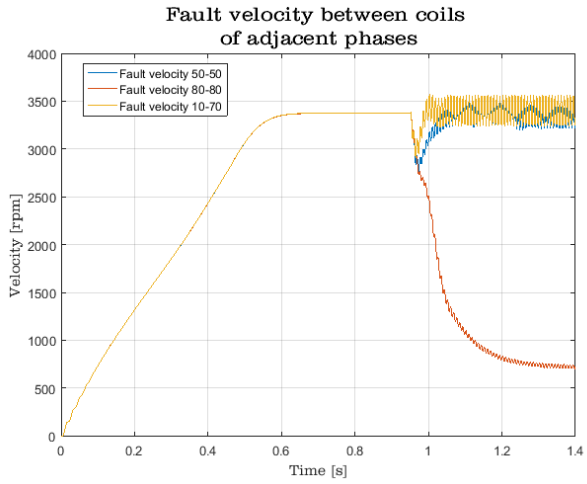

Fig 18. Speed for the fault between coils of adjacent phases.
Source: Author's own elaboration.

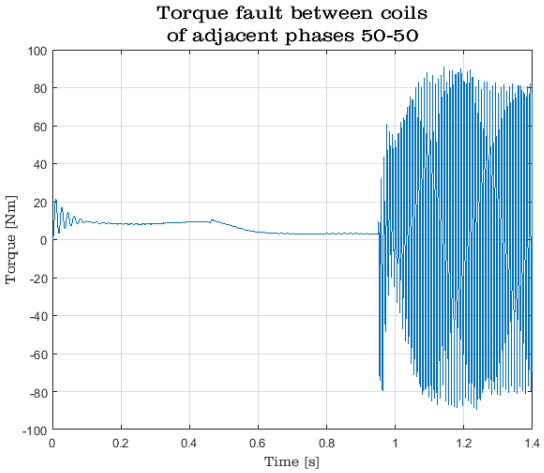

Fig 19. Torque - fault between coils of adjacent phases 50-50.
Source: Author's own elaboration.

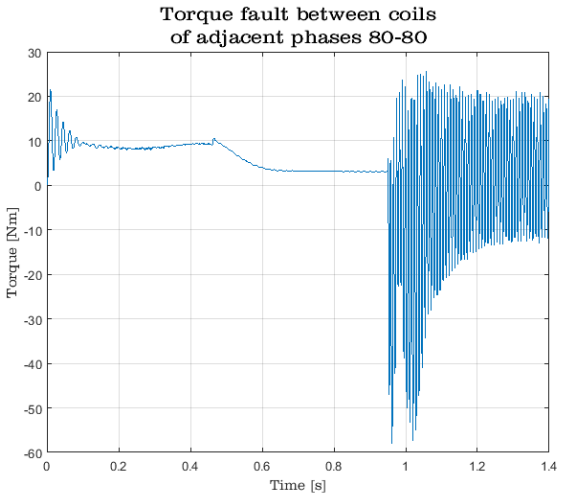

Fig 20. Torque - fault between coils of adjacent phases 80-80.
Source: Author's own elaboration.

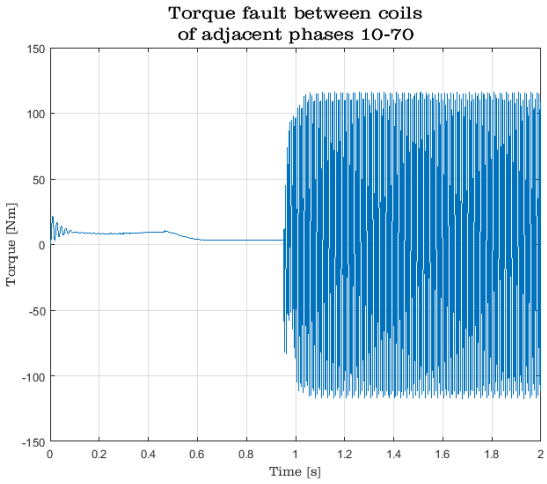

Fig 21. Torque - fault between coils of adjacent phases 10-70.
Source: Author's own elaboration.

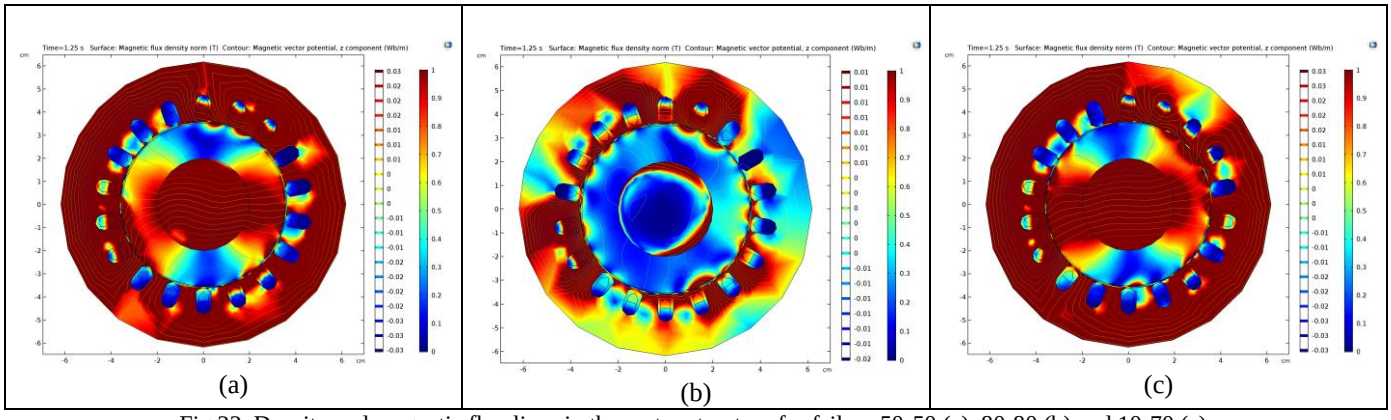

Fig 22. Density and magnetic flux lines in the motor structure for failure 50-50 (a), 80-80 (b) and 10-70 (c).
Source: Author's own elaboration.

The transition of the behavior of the voltage in the motor when it passes from normal operation to operation under failure is presented in figures 15, 16 and 17, considering the failure scenarios proposed. Figure 18 shows the behavior of the speed in a comparative manner. The behavior of the Torque is presented in figures 19, 20 and 21 correspondingly for each failure scenario. Finally, the flow distribution in the motor under fault condition is presented in figure 22.

VI. Analysis of results

Fig. 15, 16 and 17 show the supply phase voltages of the squirrel-cage motor operating with a short-circuit fault of coils of adjacent phases. In them it is evident that one of the phases is directly in short, shared characteristic for the three simulated levels of equal failure, the current per motor phase that takes a value of zero, as shown in Figures 12, 13 and 14, the difference lies in the type of response obtained, since the response of failure 80-80 is of a first order system, the other two fault current levels analyzed correspond to a second order system response. The behavior of the voltage taken by the other two phases for all the levels of severity of the simulated fault, is due to a power difference of reference to the only healthy phase, and its behavior is quite similar.

The effects of this failure on the mechanical parameters are also considerable in both speed and torque; where the speed drastically reduces its value as shown in Fig. 18 for the 50-50 fault due to the lack of complete rotation of the electromagnetic field since the machine behaves as if it had an open phase, in the case of Two other simulated fault levels result in a return to speed before failure on average but with a high level of speed ripple. For all the analyzed cases, the torque behavior represents a blockage of the rotor due to the extreme negative and positive values obtained from the torque ripple that occurs during the fault, as shown in figures 19, 20 and 21.

The results obtained from the behavior of the magnetic field density presented in figure 22, denote the number of windings affected for each case analyzed, being less the amount of field density presented for failure of 80-80 because for the most part of the windings are without circulation of fault current, the case is different for the other two simulated cases.

VII. Conclusions

The results obtained from the motor model operating without faults show a behavior similar to the real model, in variables such as speed, current and slip in the transient start state and steady state; The most significant error of the analyzed variables is the transient of the developed torque, this because the behavior of the torque is associated with electrical, mechanical and magnetic characteristics of the motor, which adds an error implied by the amount of associated variables and that they are difficult to model in the simulation used.

The results for the short circuit fault of two coils of different phase for the three simulated levels, result in a fault that causes irreparable and immediate perturbations in electrical, magnetic and mechanical fields, causing the total loss of the machine.

The fault current obtained in the simulation with COMSOL Multiphysics ® v5.3, indicates that for the case of the 50-50 and 70-10 failures a second order response is obtained and for the 80-80 fault it is obtained a response of the first order, this being the main difference between the levels of severity of the failure of adjacent phases analyzed in this article.

The finite element method using COMSOL Multiphysics ® v5.3 developed in this document is an economical, accurate and reliable alternative for the analysis of faults in electrical machines and is postulated as an alternative to conventional methods of determining parameters for faults in electrical machines.

Referencias

[1] S. Bindu and V. V Thomas, “Diagnoses of internal faults of three phase squirrel cage induction motor - A review,” in *2014 International Conference on Advances in Energy Conversion Technologies (ICAECT)*, 2014, pp. 48–54.

[2] J. Cusido Cusido, L. Romeral, J. a. Ortega, J. a. Rosero, and A. Garcia Espinosa, “Fault Detection in Induction Machines Using Power Spectral Density in Wavelet Decomposition,” *IEEE Trans. Ind. Electron.*, vol. 55, no. 2, pp. 633–643, 2008.

[3] A. Boglietti, A. Cavagnino, M. Lazzari, and M. Pastorelli, “International standards for the induction motor efficiency evaluation: a critical analysis of the stray-load loss determination,” *IEEE Trans. Ind. Appl.*, vol. 40, no. 5, pp. 1294–1301, 2004.

[4] A. M. da Silva, R. J. Povinelli, and N. A. O. Demerdash, “Induction Machine Broken Bar and Stator Short-Circuit Fault Diagnostics Based on Three-Phase Stator Current Envelopes,” *IEEE Trans. Ind. Electron.*, vol. 55, no. 3, pp. 1310–1318, 2008.

[5] A. Paz Parra, J. L. Oslinger, and J. A. Palacios, “Diagnóstico de fallas estatóricas en motores de inducción de jaula de ardilla por medio de la corriente de secuencia negativa,” *Ing. y Univ.*, vol. 18, no. 1, pp. 141–158, 2014.

[6] S. E. Pandarakone, M. Masuko, Y. Mizuno, and H. Nakamura, “Fault classification of outer-race bearing damage in low-voltage induction motor with aid of fourier analysis and SVM,” in *2018 IEEE International Conference on Industrial Technology (ICIT)*, 2018, pp. 407–412.